Pair correlation function characteristics of nearly jammed disordered and ordered hard-sphere packings

Aleksandar Donev,[1,2] Salvatore Torquato,[1,2,3,*] and Frank H. Stillinger[3]

[1]*Program in Applied and Computational Mathematics, Princeton University, Princeton, New Jersey 08544, USA*
[2]*PRISM, Princeton University, Princeton, New Jersey 08544, USA*
[3]*Department of Chemistry, Princeton University, Princeton, New Jersey 08544, USA*

We study the approach to jamming in hard-sphere packings and, in particular, the pair correlation function $g_2(r)$ around contact, both theoretically and computationally. Our computational data unambiguously separate the narrowing δ-function contribution to g_2 due to emerging interparticle contacts from the background contribution due to near contacts. The data also show with unprecedented accuracy that disordered hard-sphere packings are strictly isostatic: i.e., the number of exact contacts in the jamming limit is exactly equal to the number of degrees of freedom, once rattlers are removed. For such isostatic packings, we derive a theoretical connection between the probability distribution of interparticle forces $P_f(f)$, which we measure computationally, and the contact contribution to g_2. We verify this relation for computationally generated isostatic packings that are representative of the maximally random jammed state. We clearly observe a maximum in P_f and a nonzero probability of zero force, shedding light on long-standing questions in the granular-media literature. We computationally observe an unusual power-law divergence in the near-contact contribution to g_2, persistent even in the jamming limit, with exponent -0.4 clearly distinguishable from previously proposed inverse-square-root divergence. Additionally, we present high-quality numerical data on the two discontinuities in the split-second peak of g_2 and use a shared-neighbor analysis of the graph representing the contact network to study the local particle clusters responsible for the peculiar features. Finally, we present the computational data on the contact contribution to g_2 for vacancy-diluted fcc crystal packings and also investigate partially crystallized packings along the transition from maximally disordered to fully ordered packings. We find that the contact network remains isostatic even when ordering is present. Unlike previous studies, we find that ordering has a significant impact on the shape of P_f for small forces.

I. INTRODUCTION

Jamming in hard-sphere packings has been studied intensely in past years (see [1,2] and references therein). In this paper, we investigate the pair correlation function $g_2(r)$ of the classical three-dimensional hard-sphere system near a jamming point for both disordered (amorphous, often called random) and ordered (crystal) jammed packings. The basic approach follows that of Ref. [3], developed further for crystal packings of rods, disks, and spheres in Ref. [4]. We focus on *finite* sphere packings that are almost *collectively jammed* [5,6], in the sense that the configuration point is trapped in a very small region of configuration space around the point representing the jammed *ideal* packing [5]. Difficulties with extending the results to infinite packings will be discussed in what follows. In the ideal jammed packing particle contacts necessary to ensure jamming are exact and the particles cannot at all displace, even via collective motions. Such ideal jammed (or rigid) packings have long been the subject of mathematical inquiry [7]; however, they are not really attainable in numerical simulations where produced packings invariably have some interparticle gaps (even taking into account the unavoidable roundoff errors). It is therefore instructive to better understand the approach to this ideal

jammed state computationally and theoretically, which is the primary objective of this paper.

We choose as our main tool of exploration the shape of the venerable orientationally averaged pair correlation function $g_2(r)$ around contact. This is because this function is a simple yet powerful encoding of the distribution of interparticle gaps. In the jamming limit, it consists of a δ function due to particle contacts and a background part due to particles not in contact. As the jamming limit is approached, it is expected that the δ-function contribution will become more localized around contact. We derive the first exact theoretical model for this narrowing for isostatic packings (defined below), connecting g_2 to the probability distribution of interparticle forces P_f, and verify the relation numerically. In this work, we present computational data with unprecedented proximity to the jamming limit, clearly separating the narrowing δ-function contribution from the apparently persistent diverging background contribution. The data show that our disordered packings have an exactly isostatic contact network in the jamming limit, but with an unusual multitude of nearly closed contacts. We study the properties of the contact network and find, contrary to previous studies, no traces of polytetrahedral packing, but rather a complex local geometry, indicating that the geometric frustration due to the constraints of global jamming on the local geometry is nontrivial. Additionally, we study the evolution of the salient features of $g_2(r)$ along the transition from maximally disor-

*Electronic address: torquato@electron.princeton.edu

dered to fully ordered packings by inducing partial crystallization in the packings. We find that both $g_2(r)$ and P_f are significantly affected by crystallization; however, the contact network remains isostatic. We thus demonstrate by example that isostaticity is not synonymous with randomness.

II. THEORY

A packing of N hard spheres of diameter D in d-dimensional Euclidian space is characterized by the (Nd)-dimensional configuration vector of centroid positions $\mathbf{R} = (\mathbf{r}_1, \ldots, \mathbf{r}_N)$. Here we fix the center of mass of the packing (with periodic boundary conditions), so that in fact the configuration space is of dimension $(N-1)d$. However, we will usually neglect order-unity terms compared to N. The boundary conditions imposed determine the volume of the enclosing "container" V and the *packing* (covering) *fraction*, or *density*, ϕ.

A *jammed packing* is one in which the particle positions are fixed by the impenetrability constraints and boundary conditions [5,6]. In particular, a packing is *locally jammed* if no particle in the system can be translated while fixing the positions of all other particles, *collectively jammed* if no subset of particles can simultaneously be continuously displaced so that its members move out of contact with one another and with the remainder set, and *strictly jammed* if it is collectively jammed and all globally uniform volume-nonincreasing deformations of the system boundary are disallowed by the impenetrability constraints. Assume that a configuration $\mathbf{R}_J$ represents a collectively jammed ideal packing [5] with packing fraction ϕ_J, where there are M interparticle contacts. Next, decrease the density slightly by reducing the particle diameter by ΔD, $\delta = \Delta D / D \ll 1$, so that the packing fraction is lowered to $\phi = \phi_J (1-\delta)^d$. In this paper we restrict ourselves to an analysis which is first order in the *jamming gap* δ, $\phi \approx \phi_J (1 - d\delta)$ and focus on three-dimensional packings, $d = 3$.

A. Jamming: Configurational trapping

It can be shown that there is a sufficiently small δ that does not destroy the jamming property, in the sense that the configuration point $\mathbf{R} = \mathbf{R}_J + \Delta \mathbf{R}$ remains trapped in a small neighborhood $\mathcal{J}_{\Delta \mathbf{R}}$ around $\mathbf{R}_J$ [8]. In fact, for sufficiently small δ, it can be shown that asymptotically the set of displacements that are accessible to the packing approaches a convex *limiting polytope* (a closed polyhedron in arbitrary dimension) $\mathcal{P}_{\Delta \mathbf{R}} \subseteq \mathcal{J}_{\Delta \mathbf{R}}$ [3,4]. This polytope is determined from the linearized impenetrability equations

$$\mathbf{A}^T \Delta \mathbf{R} \leq \Delta \mathbf{l}, \tag{1}$$

where $\mathbf{A}$ is the (dimensionless) *rigidity matrix*[1] of the pack-

FIG. 1. (Color online) The polytope of allowed displacements, $\mathcal{P}_{\Delta \mathbf{R}}$, for a locally jammed disk (light shade) trapped among three (left) or six (right, as in the triangular lattice) fixed disks (dark shade). The exclusion disks (dashed lines) of diameter twice the disk diameter are drawn around each of the fixed disks, along with their tangents (solid lines) and the polytope $\mathcal{P}_{\Delta \mathbf{R}}$ they bound (dark). For the isostatic case on the left this polytope is a triangle (a *simplex* in two dimensions) and a hexagon for the *hyperstatic* case on the right.

ing and $\Delta \mathbf{l}$ is the set of interparticle gaps [5]. In our case $\Delta \mathbf{l} = \Delta D \mathbf{e}$, where $\mathbf{e}$ is a vector of M elements all equal to 1. We can therefore focus on the normalized polytope $\mathcal{P}_{\mathbf{x}} : \mathbf{A}^T \mathbf{x} \leq \mathbf{e}$, which can be scaled by a factor of δD to obtain $\mathcal{P}_{\Delta \mathbf{R}}$. Examples of such polytopes for a single disk are shown in Fig. 1. A troublesome aspect, discussed in Ref. [3], is that infinite packings can never be jammed in the above sense unless $\delta = 0$, due to the appearance of unjamming mechanisms involving collective density fluctuations. Nevertheless, computational studies indicate that macroscopic properties derived using this polytope-based approach do not depend on N, even as $N \to \infty$.

The polytope $\mathcal{P}_{\mathbf{x}}$ is necessarily bounded for a collectively jammed configuration, which implies that $\mathbf{A}$ is of full rank [5] and that the number of faces bounding $\mathcal{P}_{\mathbf{x}}$—i.e., the number of interparticle contacts M—is at least one larger than the dimensionality d_{CS} of the configuration space,[2] $M \geq d_{CS} + 1$. For collective jamming [5] the boundary conditions are fixed and with periodic boundary conditions there are d trivial translational degrees of freedom, so $d_{CS} = (N-1)d$. If hard-wall boundary conditions are employed, then $d_{CS} = Nd$ and one should also count contacts with the hard walls among the M constraints. For strict jamming [5] the boundary is also allowed to deform and this introduces additional degrees of freedom. For example, with periodic boundary conditions a symmetric nonexpansive macroscopic strain tensor is added to the configuration parameters, giving $d_{CS} = (N-1)d$

---

[1] This matrix combines geometrical information with the topological connectivity information contained in the node-arc *incidence matrix* of the graph representing the contact network of the packing. Namely, $\mathbf{A}$ has Nd rows, d rows for each particle, and M columns, one for each contact. The column corresponding to the contact between particles i and j is nonzero only in the rows corresponding to

the two particles, and contains the unit surface normal vector at the point of contact [5].

[2] The additional $+1$ comes because we are considering inequality constraints, rather than equalities. One can also think of this extra degree of freedom as representing the density—i.e., the size of the particles. For example, looking at the left panel of Fig. 1 we see that at least three linear inequalities are necessary to bound a polytope in two dimensions.

$+d(d-1)/2+(d-1)$ degrees of freedom.[3] *Isostatic* packings are jammed packings which have the minimal number of contacts: Namely, for collective jamming,

$$M = \begin{cases} 2N-1 & \text{for } d=2, \\ 3N-2 & \text{for } d=3, \end{cases} \qquad (2)$$

and for strict jamming,

$$M = \begin{cases} 2N+1 & \text{for } d=2, \\ 3N+3 & \text{for } d=3, \end{cases} \qquad (3)$$

with periodic boundary conditions. Packings having more contacts than necessary are *hyperstatic*, and packings having fewer contacts are *hypostatic* (for sphere packings these cannot be jammed in the above sense). For the trivial example of local jamming and $N=1$, all particles but one are frozen in place and the free particle must have at least $d+1$ contacts. Figure 1 shows the polytope $\mathcal{P}_{\Delta\mathbf{R}}$ for a locally jammed disk, for both an isostatic and a hyperstatic case. In this work, we focus on collectively jammed packings, since strictly jammed packings are hard to produce with existing algorithms. For sufficiently large disordered systems, the differences between collective and strict jamming are expected to be insignificant [9].

We now consider adding thermal kinetic energy to this nearly jammed hard-sphere packing. While the system may not be ergodic and thus not in thermodynamic equilibrium, especially if considering disordered packings [10], one can still define a suitable macroscopic pressure by considering only time averages as the system executes tightly confined motion around the *particular* configuration $\mathbf{R}_J$. In a sense, the configuration will explore the interior of $\mathcal{P}_{\Delta\mathbf{R}}$ and ergodicity is restored if one restricts the configurational space to $\mathcal{P}_{\Delta\mathbf{R}}$. For a finite packing, which is sufficiently close to its jamming point, the time-averaged properties will always be well defined. Since the available (free) configuration volume scales in a predictable way with the jamming gap, $|\mathcal{P}_{\Delta\mathbf{R}}| = (\delta D)^{Nd}|\mathcal{P}_{\mathbf{x}}|$, one can show that the reduced pressure is asymptotically given by the free-volume equation of state [3],

$$p = \frac{PV}{NkT} = \frac{1}{\delta} = \frac{d}{(1-\phi/\phi_J)}. \qquad (4)$$

Relation (4) is remarkable, since it enables one to accurately determine the true jamming density of a given packing even if the actual jamming point has not yet been reached, just by measuring the pressure. We later numerically confirm the validity of Eq. (4) in the vicinity of the jamming point.

B. Jamming: Interparticle forces

As the particles travel around $\mathbf{R}_J$ and the configuration explores $\mathcal{P}_{\Delta\mathbf{R}}$, one can average the exchange of momentum between any two pairs of particles which share a contact in the jammed limit (i.e., whose contact forms a face of $\mathcal{P}_{\mathbf{x}}$),

hereafter referred to as *first neighbors*, to obtain an average interparticle *force* (momentum transfer per unit time or impulse [11]), as detailed in Ref. [12]. This kind of method for measuring interparticle forces has previously been used in work on dense granular flows [11]. The vector of collisional forces $\mathbf{f}$ compares directly to the intergrain force networks which have been the subject of intense experimental and theoretical study in the field of granular materials [13–16]. These forces are in local equilibrium,

$$\mathbf{Af} = \mathbf{0}, \qquad (5)$$

where we take the forces to be non-negative,[4] $\mathbf{f} \geq \mathbf{0}$, and normalize them to have a unit average, $\bar{f} = \mathbf{e}^T\mathbf{f}/M = 1$, in the tradition of the granular media literature. Our numerical investigations indicate that indeed the set of time-averaged collisional forces approaches local equilibrium as the time horizon T of the averaging increases, in a inverse-power-law manner, $\|\mathbf{Af}\| \sim T^{-1}$. We can therefore obtain interparticle forces relatively accurately given sufficiently long molecular dynamics runs. While Eq. (5) will have a unique solution if and only if the contact network of the packing is isostatic, even for hyperstatic packings, such as the fcc packing, the equilibrium set of forces should be unique. In fact, one can prove that the force between two particles will be proportional to the surface area of the face of $\mathcal{P}_{\mathbf{x}}$ formed by the contact in question.

It is interesting to observe that if one has an *arbitrary* point $\Delta\mathbf{R} \in \mathcal{P}_{\Delta\mathbf{R}}$, the interparticle gaps due to nonzero jamming gap will be $\Delta\mathbf{l} \approx \mathbf{A}^T\Delta\mathbf{R} - \delta D\mathbf{e}$, so that

$$\mathbf{f}^T\Delta\mathbf{l} \approx (\mathbf{Af})^T\Delta\mathbf{R} - MD\delta = -MD\delta. \qquad (6)$$

Equation (6) enables one to determine how far from the jamming density a packing is without actually reaching the jamming point. This can be a useful alternative to using Eq. (4) when the hard-sphere pressure is not available, but interparticle forces are, such as, for example, with packings generated by algorithms using stiff "soft" spheres [17].

As already pointed out, hypostatic packings cannot be jammed. However, it is possible for a hypostatic packing to be *locally maximally dense*, in the sense that no continuous motion of the particles can increase the density to first order. In other words, the particles must first move and unjam (which must be possible for a hypostatic sphere packing) before the density can increase. In particular, a packing of contacting particles for which a set of interparticle forces $\mathbf{f}$ in equilibrium exists is locally maximally dense. In a sense, the interparticle forces resist further increase of the density. As we discuss later, our packing generation algorithm sometimes terminates with such packings since it tries to continually increase the density.

C. Pair correlation function around contact

We now turn to the central subject of this work: the shape of the (orientation-averaged) pair correlation function $g_2(r)$

---

[3] Here $d(d-1)/2$ gives the number of off-diagonal strain components and $d-1$ comes from the number of diagonal components (d) whose sum is constrained to be nonpositive (−1).

[4] This sign convention is in agreement with the granular media literature, but opposite to our own preferred notation [5].

for small jamming gaps. In particular, we will focus on interparticle distances r that are very close to D. We express $g_2(l)$ in terms of the non-negative *interparticle gaps* $l=r-D$. The polytope picture above says that only the M first-neighbor particle pairs will contribute to the shape of $g_2(l)$ right near contact—i.e., for gaps up to l_{max}, where l_{max} is the largest distance from the centroid of $\mathcal{P}_{\Delta \mathbf{R}}$ to one of its faces. This contribution will become a δ function in the jamming limit. Particle pairs not in contact will not contribute to $g_2(l)$ until gaps larger than the minimal farther-neighbor gap l_{FN}, and for now we will implicitly assume that $l_{FN} \gg l_{max}$, so that there is a well-defined δ-*function region* $g_2^{(\delta)}(l) \equiv g_2(l \ll l_{FN})$. This δ-function region has previously been investigated theoretically for crystal packings, primarily [4]. In this work, we derive exact theoretical expressions for this region for isostatic packings, as well as numerically study vacancy-diluted fcc crystals and partially crystallized packings.

Isostatic packings

We first focus on the probability distribution for observing an interparticle gap l, $P_l(l)$, which is related to $g_2^{(\delta)}(l)$ via a simple normalization factor. The contribution $\tilde{P}(l)$ from a specific contact is determined from the area $\tilde{S}(l)$ of the cross section of $\mathcal{P}_{\mathbf{x}}$ with a plane parallel to the face corresponding to the contact and at a distance l from the face, $\tilde{P}(l) \sim \tilde{S}(l)$ [4]. The critical observation we make is that for an isostatic contact network, $\mathcal{P}_{\mathbf{x}}$ is a *simplex*[5] and thus immediately we get $\tilde{S}(l) \sim [(h-l)/h]^M$, where h is the height of the simplex corresponding to this particular face, $h=M|\mathcal{P}_{\mathbf{x}}|/S$, $S=\tilde{S}(0)$. After normalization of $\tilde{P}(l)$ and averaging over all interparticle contacts, we obtain that

$$P_l(l) = \int_{h=l}^{\infty} \frac{M}{h} \left[1 - \frac{l}{h}\right]^M P_h(h)dh,$$

which shows that if we know the distribution P_h of heights for the simplex $\mathcal{P}_{\mathbf{x}}$ or, equivalently, the distribution of surface areas S of the faces of the polytope $P_S(S)$, we would know P_l and thus $g_2^{(\delta)}$.

Since the interparticle force $f \sim S$, we see immediately that the distribution of face areas is equivalent to the distribution of interparticle forces $P_f(f)$, and in fact it is easy to derive that

$$h/\Delta D = 1 + \frac{\mathbf{e}^T \mathbf{f}}{f} \approx \frac{M}{f},$$

which gives, in the limit $M \to \infty$,

$$P_l(l) = \int_{f=0}^{M/l} \frac{f}{\Delta D}\left[1 - \frac{lf}{M\Delta D}\right]^M P_f(f)df$$

$$\approx \frac{1}{\Delta D}\int_0^{\infty} fP_f(f)\exp(-fl/\Delta D)df$$

$$= \frac{1}{\Delta D}\mathcal{L}_{l/\Delta D}[fP_f(f)],$$

where $\mathcal{L}_s$ denotes the Laplace transform with respect to the variable s. We have the normalization condition $\int_0^{\infty}P_l(l)dl = 1$ and additionally

$$DP_l(0) = \frac{D}{\Delta D}\int_0^{\infty} fP_f(f)df = \frac{D}{\Delta D} = p.$$

If we now relate $P_l(l)$ to $g_2^{(\delta)}(l)$,

$$g_2^{(\delta)}(l) = \frac{2MV}{4\pi D^2 N^2}P_l(l) = \frac{\bar{Z}D}{24\phi}P_l(l),$$

where $\bar{Z}=2M/N=2d=6$ is the *mean coordination number*, we obtain the central theoretical result

$$g_2^{(\delta)}(l) = \frac{p}{4\phi}\mathcal{L}_{l/\Delta D}[fP_f(f)]. \tag{7}$$

D. Classification of jammed packings

Jammed hard-sphere packings can be classified based on their density ϕ. However, such a classification is clearly not sufficient in order to distinguish between *ordered* and *disordered* (often called random, despite the shortcomings of such terminology) packings [18,19]. In fact, packings can have various degrees of order in them, and for hard-sphere packings the dominant form of ordering is crystallization into variants of the fcc lattice. We can use a hypothetical scalar order metric ψ to measure the amount of order in a packing, such that $\psi=1$ corresponds to fully ordered (for example, the perfect fcc crystal) and $\psi=0$ corresponds to perfectly disordered (Poisson distribution of sphere centers) packings. Very large jammed packings are thus classified based on their position in the density-disorder (ϕ-ψ) plane, as sketched in Fig. 2, as taken from Ref. [18]. A state of special interest is the MRJ state, representing the collection of *maximally random jammed* packings, believed to be closely related to the traditional but ill-defined concept of random close packing (RCP) in three dimensions, if strict jamming is considered, and to have a density of about $\phi \approx 0.64$ in three dimensions.[6] Additionally, the perfect fcc crystal and variants thereof correspond to the most dense jammed packing, with $\phi \approx 0.74$. This work will focus on these two points in the ϕ-ψ plane. However, it is possible to produce packings with intermediate amounts of order and densities—for example, by allowing partial crystallization.

---

[5]A simplex is a closed convex polytope that has $\nu+1$ faces and $\nu+1$ vertices in ν-dimensional space (i.e., a triangle in two or a tetrahedron in three dimensions). Our definition of isostatic thus implies that $\mathcal{P}_{\mathbf{x}}$ is a simplex.

[6]Contrary to popular belief, the traditional concept of RCP does not have a two-dimensional analog for monodisperse disks [9,20].
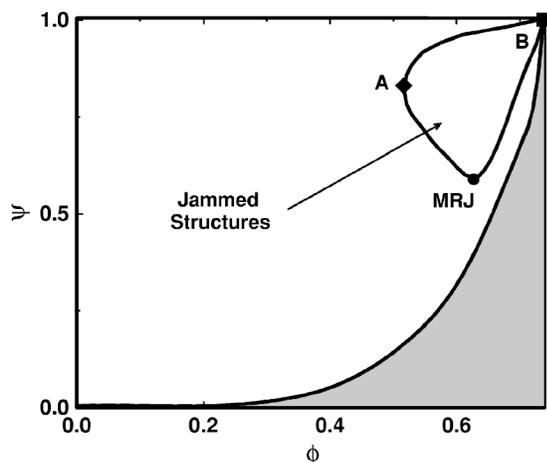
FIG. 2. A highly schematic plot of the subspace in the density-disorder (ϕ-ψ) plane where strictly jammed three-dimensional packings exist. Point A corresponds to the lowest-density jammed packing, and it is intuitive to expect that a certain ordering will be needed to produce low-density jammed packings. Point B corresponds to the most dense jammed packing. Point MRJ represents the maximally random jammed state. This is the most disordered jammed packing in the given jammed category (locally, collectively or strictly jammed). We conjecture that the Lubachevsky-Stillinger packing algorithm [21,22] typically produces packings along the right (maximally dense) branch, and we do not know of an algorithm that produces packings along the left (minimally dense) branch.

III. COMPUTATIONAL RESULTS

We use event-driven molecular dynamics [12] as the primary computational tool for our investigations. This enables us to perform exact molecular dynamics on hard-particle packings very close to the jamming point, which is not possible with traditional time-driven molecular dynamics algorithms. The algorithm monitors a variety of properties during the computational run, including the "instantaneous" pressure, as calculated from the total exchanged momentum in all interparticle collisions during a certain short time period Δt. By allowing the shape of the particles to change with time—for example, by having the sphere diameter grow (shrink) uniformly at a certain (possibly negative) expansion rate $dD/dt=2\gamma$—one can change the packing density. If the change is sufficiently slow, the system will be in approximate (metastable) equilibrium during the densification and one can rather effectively gather quasiequilibrium data as a function of density.

Event-driven molecular dynamics (see Ref. [12] and references therein) in which the particles (quickly) grow in size in addition to their thermal motion at a certain expansion rate, starting from a random (Poisson) distribution of points, produces a jammed state with a diverging collision rate. This is the well-known Lubachevsky-Stillinger (LS) packing algorithm [21,22], which we have used and modified [12] to generate all the disordered hard-sphere packings for this study. During the initial stages, the expansion has to be fast to suppress crystallization and maximize disorder [19], and delaying further discussion to later sections, we will assume
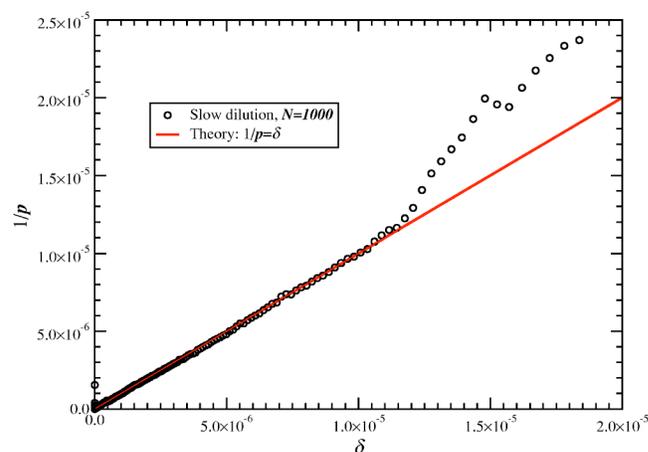
FIG. 3. (Color online) The inverse of the "instantaneous" (averaged over several hundred collisions per particle) pressure of a nearly jammed (isostatic) packing of 1000 particles, as it is slowly diluted (using a negative expansion rate for the particles in the molecular dynamics algorithm $\gamma=-10^{-5}$) from $\phi_J \approx 0.627$ until an unjamming particle rearrangement occurs. Up to this occurrence, the free-volume theoretical relation $p=\delta^{-1}$ is satisfied to very high accuracy. There is a short transient region during the initial equilibration of the packing. Rattlers have been removed from the packing.

that the disordered packings used in this study are representative of the MRJ state. It is important to note that the algorithm typically produces packings that have *rattling* particles—i.e., particles that do not have true contacts with particles in the jammed *backbone*[7] of the packing and can be removed without affecting the jamming category of the final packing. We will discuss procedures for the identification of such rattlers in what follows.

To our knowledge, no verification of the exactness of Eq. (4) for disordered packings exists in the literature. The perfect fcc crystal is stable until rather low densities, and the pressure seems to be rather accurately predicted by the free-volume approximation in a wide range of densities around close packing. This has been observed in the literature and a suitable corrective term was determined [23]. However, for disordered packings, previous studies have identified a coefficient smaller than 3 in the numerator: namely, 2.67 [24,25]. In Fig. 3, we numerically confirm the validity of Eq. (4) with very high accuracy for disordered packings. In Fig. 4, we show the change of the coefficient (the constant volume heat capacity in units of Nk) $C=(1-\phi/\phi_J)p$ with density. Agreement with the theoretical $C=d=3$ is observed sufficiently close to the jamming point, but with rapid lowering of the coefficient from 3 away from the jamming point. This is because for sufficiently large jamming gaps, contacts other than the M true contacts start contributing to the collisions, and the polytope-based picture we presented so far does not apply exactly. We demonstrate this in Fig. 4 by showing the number of contacts which participate in collisions (*active contacts*) as the jamming point is approached. Our investiga-

---

[7]The backbone is formed by the collection of particles that participate in the jamming force network [5].
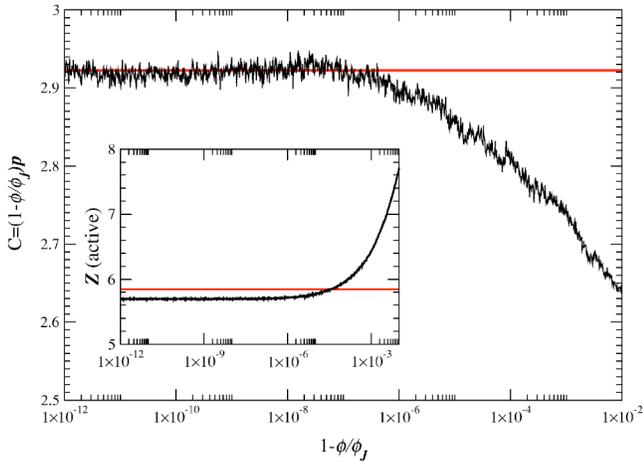
FIG. 4. (Color online) The coefficient C during a typical slow densification (expansion rate is 10^{-4}) of a 10 000–particle system, starting from an equilibrated liquid at $\phi=0.5$ up to jamming. The final packing has 259 rattlers, so the expected coefficient is $3 \times 0.9741 \approx 2.92$, a value which is shown with a red line. It is clear that close to the jamming point Eq. (4) is very accurate, but a marked lowering from a coefficient of 3 is seen for pressures lower than about 10^6, likely explaining the coefficient 2.67 reported in works of Speedy [24,25]. The inset shows the estimated "collisional" coordination, defined as the average number of different particles that a particle has collided with during a time interval of about 100 collisions per particle, during the same densification. The expected number $6 \times 0.9741 \approx 5.85$ is shown (this number is not asymptotically reached exactly since some of the M contacts do not participate in collisions frequently enough to be registered during the time interval used), and we see that as many as eight contacts per particle are active at sufficiently large jamming gaps.

tions indicate that previous studies did not examine at the range of densities appropriate for the theory presented above and did not properly account for the rattlers.

A. Disordered packings

We have verified in previous publications that LS packings are typically collectively jammed [9] using a testing procedure based on linear programming [5]. Unfortunately, the linear programming library used in the implementation cannot really achieve the kind of numerical accuracy that we require in this work, specifically that for packings which are jammed almost to within full numerical precision ($\delta=10^{-15}-10^{-12}$). Additionally, it cannot handle three-dimensional packings of more than about 1000 particles. Another test for jamming, which we have found to be reliable for the purposes of this work, is to take the final packing produced by the LS procedure and then run standard event-driven molecular dynamics on it for long periods of time (on the order of thousands to hundreds of thousands of collisions per particle) and monitor the "instantaneous" pressure. If the packing is jammed, this pressure will be stable at its initial value. However, if the packing is not truly jammed, we have observed that the pressure slowly decays with time; the slower the "pressure leak," the more "jammed" the initial packing is, as illustrated in Fig. 5. Similar observations are
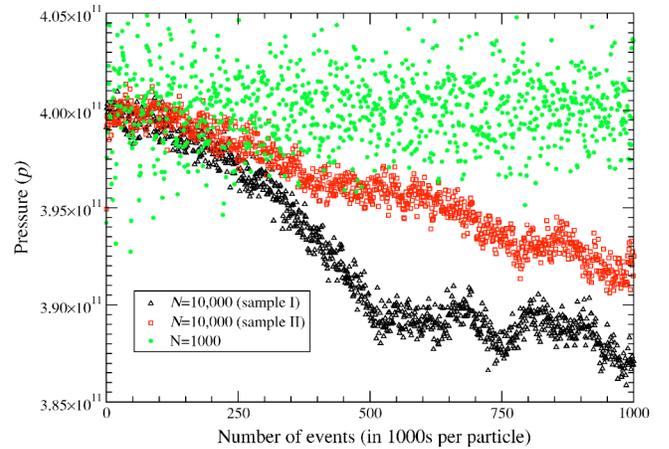
FIG. 5. (Color online) The short-term ("instantaneous") pressure versus number of events (mostly binary collisions) processed by the molecular dynamics algorithm [12], corresponding to a total run of about half a million collisions per particle. For the 1000-particle packing the pressure is stable, but for the larger packings a systematic pressure leak is observed.

made in Ref. [24]. In addition, we track the average particle displacement (from the initial configuration) and check to see if there is a systematic drift with time away from the initial configuration. The two tests always agreed: A pressure leak always corresponds to a systematic drift away from the initial configuration.

We have observed that LS packings densified to within numerical capability only pass this rigorous jamming test of having no pressure leak if during the final stages of the LS densification the expansion rate is very small compared to the average thermal velocity (maintained constant via a velocity rescaling thermostat [12]) of the particles (about five orders of magnitude or less). Similar observations are made in Ref. [24]. If the expansion rate is too fast, we have found that the packings jam in slightly hypostatic configurations, where there are not enough particle contacts to ensure jamming. In particular, some particles have two or three contacts (and of course rattlers are present). In order for a set of balanced forces to exist (which as we discussed is a necessary condition for a packing to be locally maximally dense) when a particle has fewer than four contacts, these contacts must be in a degenerate geometric configuration: namely, three coplanar or two collinear contacts. We have indeed verified that this is what happens in the hypostatic packings produced by the LS algorithm. The number of such geometric peculiarities increases with increasing expansion rate and also for more ordered packings, as we discuss later.

We illustrate the progress of the densification during the final stages of the algorithm in Fig. 6. The figure shows, for several snapshots of the packing during the densification, the *cumulative coordination number*

$$Z(l) = \frac{N}{V} \int_{r=D}^{D+l} 4\pi r^2 g_2(r) dr = 24\phi \int_{r=D}^{D+l} \left(\frac{r}{D}\right)^2 g_2(r) \frac{dr}{D},$$
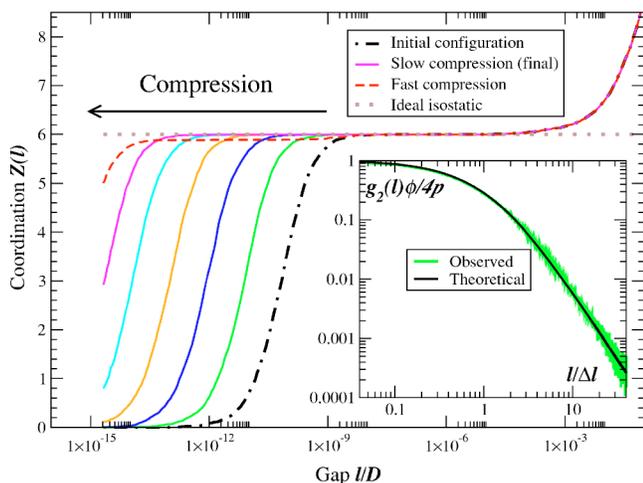
FIG. 6. (Color online) The cumulative coordination $Z(l)$ [i.e., the integral of $g_2(l)$] as a function of the gap tolerance l, for a sequence of snapshots of a 1000-particle packing during the final compression stages of the LS algorithm. Each snapshot is shown with a separate solid curve and only the last one is labeled in the figure legend. For a sufficiently slow expansion (expansion rate is 10^{-5} times the average thermal velocity), the packing is clearly seen to jam in an isostatic configuration. A subisostatic configuration is found for fast expansion (expansion rate is comparable to the thermal velocity). The inset shows the properly normalized derivative of $Z(l)$, right around contact, along with a comparison to our semi-theoretical prediction for $g_2^{(\delta)}(l)$, for a packing with $\delta = 2.5 \times 10^{-12}$.

i.e., the average number of particles within a gap l from a given particle. We we will often use this quantity instead of $g_2(l)$. With unprecedented clarity, a clear separation is seen between the δ-function contribution $Z^{(\delta)}(l)$, which becomes more localized around contact, and the background increase in the mean coordination from the isostatic contact value of $\bar{Z} = 6$, which remains relatively unaffected by the densification. For small packings ($N = 1000$), the value of $Z(l)$ is fixed at 6 for a remarkably wide range of gaps, as much as nine orders of magnitude for the final packings. Fast densification is seen to lead to subisostatic packings in Fig. 6, leaving a certain fraction of the contacts "open." Stopping the expansion invariably leads to a decay of the macroscopic pressure for such subisostatic packings.

By using heuristic strategies, we were able to find (slow) densification schemes which produced packings which are indeed ideally jammed within almost full numerical precision, at least for packings of $N = 1000$ particles or less. In fact, the plateau in $Z(l)$ was at exactly (up to a single contact) an isostatic number of contacts, $M = 3N - 2$, for all the packings produced via a carefully guided LS algorithm. It is essential that here N is the number of particles in the jammed backbone of the packing [5]; i.e., rattlers [22] with fewer than two contacts have been removed from the packing. It seems that the algorithm produces packings with about 2.2% rattlers, and so the density of the disordered packings we look at is typically $\phi \approx 0.625 - 0.630$, rather than the widely known $\phi \approx 0.64$. Despite a concentrated effort and lots of expended CPU time, we have been unable to achieve true

isostaticity for 10 000–particle packings.[8] This is illustrated in Fig. 5, where it is clearly seen that the pressure in the large packings does not remain constant over long periods of time (about 10^6 collisions per particle). It is therefore not strictly justified to consider these packings within the framework of ideal jammed packings that we have adopted here. However, it is readily observed that over finite and not too long time intervals (for example, several thousands of collisions per particle), the large packings conform to the predictions of the theory developed here. In particular, the collisional forces form a balanced force network with essentially the same $P_f(f)$ as the truly jammed smaller packings, and the pressure is given by Eq. (4) with very high accuracy, where δ can be determined, for example, via Eq. (6). We have observed no systematic differences in any of the correlation functions or distributions between the jammed isostatic packings with 1000 particles and the ones with 10 000 particles, other than the better binning resolution of the larger packings and larger statistical variability among the small packings. Results given in subsequent sections will indicate that the fact we could not achieve true jamming for very large packings is an inherent property of the kinds of packings we consider, rather than a failure of the simulation method. We therefore believe it is justified to use the larger packings for certain analysis where better statistics are needed.

The main goal of this work is to explore and explain Fig. 6 and, in particular, to investigate both the "δ-function," or *contact*, contribution $g_2^{(\delta)}$, which should integrate to produce the isostatic average coordination $\bar{Z} = 2M/N = 6$, and the "background" or *near-contact* $g_2^{(b)}$, for gaps from about $100\delta D - 10^{-1}D$. This latter one has already been observed in an experimental study of hard spheres [26] and in computational studies of stiff "soft" spheres [17,27]. These various studies find a nearly square-root divergence, $g_2^{(b)}(l) \sim 1/\sqrt{l}$, and Ref. [27] observes that this is an integrable divergence and thus clearly separate from the δ function. Our results, shown in Fig. 6, are an unambiguous and precise separation of the two pieces of the pair correlation function around contact near jamming. Our numerical data have precision ($\delta < 10^{-13}$) not previously attained, since such proximity to ideal jammed hard-sphere packings can only be achieved in a true hard-sphere algorithm, and at present only event-driven molecular dynamics seems to provide the required numerical robustness. It is rather interesting that although graphs showing the hard sphere $g_2(l)$ in the literature have clearly demonstrated a divergence in $g_2(l)$ near contact for at least three decades [28], this seems to never have been clearly documented or investigated. We are led to believe that researchers were under the false impression this divergence is a signature of the δ-function contribution and thus expected it to further narrow and disappear at true jamming.

1. δ-function (contact) contribution

We first verify that our theory correctly predicts the shape of $g_2^{(\delta)}(l)$. In order to verify relation (7) numerically, a form

---

for $P_f(f)$ is needed. Force networks in particle packings have been the subject of intense theoretical and experimental interest [13,15,16,29,30], and it has been established that P_f decays exponentially at large forces for a variety of models. The behavior of P_f for small forces has not been agreed upon, the central question being whether the infinite-system-limit $P_f(0)$ is nonzero. No theoretical model has been offered yet that truly answers this question. We note that a recent model reproduces all of the major characteristics of P_f that we observe, including a positive $P_f(0)$, even though it is presently restricted to two dimensions [31]. Part of the difficulty is that the answer likely depends not only on the system in question, but also on the definition of f. In a true ideal collectively jammed isostatic packing, which is necessarily finite, all interparticle forces *must* be strictly positive and, in fact, are determined uniquely through Eq. (8),

$$\mathbf{f} = \begin{bmatrix} \mathbf{A} \\ \mathbf{e}^T \end{bmatrix}^{-1} \begin{bmatrix} \mathbf{0} \\ 1 \end{bmatrix},$$ (8)

without any mention of interparticle potentials or influence of external fields or loads like gravity or thermal dynamics. The limiting probability distribution of these interparticle forces as the packing becomes larger, if it exists, can be positive at the origin, indicating that finite but large packings have limiting polytopes with a few extremely small faces or, equivalently, are very elongated along certain directions. We have numerically studied the form of $P_f(f)$ for almost jammed random packings of $N=1000$ and $N=10\,000$ spheres by using molecular dynamics to observe the collisional forces between first neighbors and also by directly using Eq. (8) for the smaller packings[9] (this offers better accuracy for small forces). The results are shown in Fig. 7. We clearly see a peak in $P(f)$ for small forces, as observed in the literature for jammed packings of soft particles [29], and it appears that there is a finite positive probability of observing zero interparticle force. We will return to this point later.

The observed $P_f(f)$ can be well fitted for medium and large forces by $P_f(f)=(Af^2+B)e^{-Cf}$, with a small correction needed to fit the small-force behavior, as used in Fig. 7. This small correction has a negligible impact on the Laplace transform of $fP_f(f)$, and in fact a very good approximation to $g_2^{(\delta)}(l)$ in Eq. (7) is provided by just using

$$\mathcal{L}_x[fP_f(f)] = \frac{6A}{(x+C)^4} + \frac{B}{(x+C)^2}.$$ (9)

In the inset in Fig. 6, we show a comparison between the $g_2^{(\delta)}(l)$ we observe computationally and the one given by Eqs. (7) and (9) and the empirical fit to $P_f(f)$ in Fig. 7. An essentially perfect agreement is observed. Our focus here is on small forces; however, we do wish to note that our data cannot confidently rule out a Gaussian component to P_f for large forces and that a slight quadratic component does seem to be visible when $P_f(f)$ is plotted on a log-log plot.

---

[9]Efficiently inverting the rigidity matrix for very large three-dimensional packings is a rather challenging numerical task which we have not yet tackled.
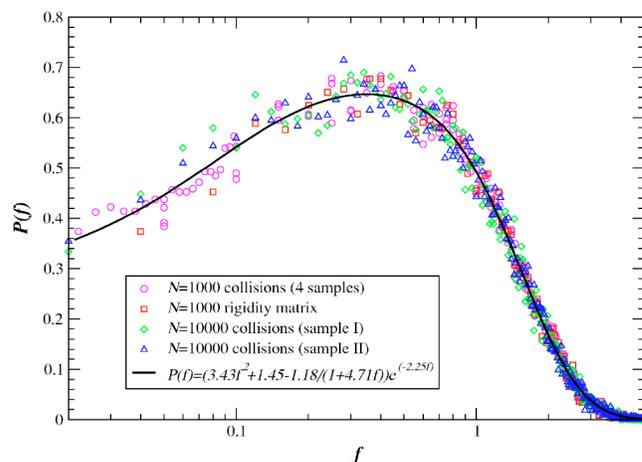
FIG. 7. (Color online) Computational data on the interparticle force distribution along with the best fit we could achieve. Packings of both 1000 and 10 000 particles, using either molecular dynamics to average the collisional forces or inversion of the rigidity matrix, were used, consistently producing the same probability distribution. Comparison to other data in the granular-media literature is beyond the scope of this work.

2. Near-contact contribution

In Fig. 8 we investigate the near-contact contribution to $g_2(l)$. We have found that $Z^{(b)}(l)$ has a power-law behavior over a surprisingly wide range of gaps, up to the first minimum of g_2 at $l \approx 0.25D$, $Z^{(b)}(l) \approx 11(l/D)^{0.6}$, as shown in the figure. Note that this range is too wide for

$$g_2^{(b)}(x) = \frac{1}{24\phi(1+x)^2} \frac{dZ^{(b)}(x)}{dx}$$

to be a perfect power law, where $x=l/D$, as used to fit numerical data in other studies (which have not investigated
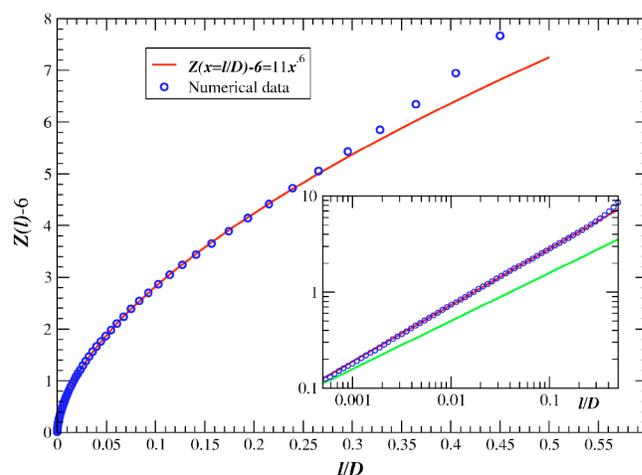
FIG. 8. (Color online) The near-contact $Z^{(b)}(l)$ for a nearly jammed 10 000–particle packing, along with a power-law fit for small gaps, shown in both a linear-linear scale and a log-log scale (inset). In this inset we also show a line with slope 0.5 (i.e., a square-root dependence), which is clearly inconsistent with the numerical data.

nearly as wide a range of gaps as we do here) [27,26]. The observed exponent is clearly distinguishable from an inverse square-root divergence in $g_2^{(b)}(l)$, as proposed in the literature [27], and it is consistent with the experimental exponents reported in Ref. [26]. Our study has higher statistical accuracy than previously realized; however, it is not clear if there are not also systematic effects due to the different protocols used to prepare the packings in studies such as Ref. [27].

We do not have a theoretical explanation for this functional behavior of $Z^{(b)}(l)$; however, the remarkable quality of the fit in Fig. 8 hints at the possibility of a (simple) scaling argument. Some simple observations can be made by assuming that

$$Z(x) = \bar{Z} + ax^{1-\alpha} \quad \text{for } 0 < x \leqslant \beta, \qquad (10)$$

where α is an exponent $0 \leqslant \alpha \leqslant 1$ and $\beta < 1$ determines the extent of this power-law dependence. The corresponding pair correlation function of course exhibits an inverse power-law divergence with exponent α, except when $\alpha = 1$, when it is identically zero.[10] The exponent α clearly will depend on the amount of order present in the packing—i.e., the position of the packing in the density-order diagram of Fig. 2. We expect that it will increase with increasing order, since $\alpha \to 0$ would indicate a constant $g_2(l)$ near contact, a signature of the ideal gas, while $\alpha \to 1$ would indicate a clear distinction between the first and second shells of neighbors (i.e., a wide range of gaps with very few contacts) typical of crystal packings. Under the assumption that a power-law divergence in g_2 is appropriate, an intermediate value of α between 0 and 1, as we find numerically, is therefore expected. Some bounds on the range of possible α can be obtained from bounds on $Z(x)$ derived from geometric constraints [for example, $Z(x) < 13$ for a certain range of x since the sphere kissing number is 12 in three dimensions], but the exact value is not simple to predict.[11]

3. Away from contact: Split-second peak

Although the primary focus of this work is on the behavior of $g_2(r)$ around contact, it is instructive to also look at the split-second peak of the pair correlation function, shown for a sample of packings of 10 000 particles in Fig. 9. Only two clear discontinuities are seen: one at exactly $r = \sqrt{3}D$ and one at $r = 2D$. The latter is very clearly asymmetrical, with a sharp decrease in g_2 at $r = 2D^+$. Although the first discontinuity is less pronounced and statistics are not good enough to unambiguously determine its shape, it appears that it also has the same shape as the second discontinuity, only of smaller magnitude. The split-second peak is of great importance because it is a clear signature of the strong local order in the

---

[10]Note that $g_2^{(b)}(x)$ cannot have a simple-pole divergence since this would lead to a logarithmic divergence in $Z^{(b)}(x)$, which must be finite for all finite x.

[11]The three parameters α, β, and a are thus not independent of one another. For example, requiring that $g_2^{(b)}(x) > 1$ and $Z(x) < 12$ for $0 < x \leqslant \beta$ gives the weak constraints $a(1-a) > 24\phi\beta^2(\beta-1)^\alpha$ and $a(\beta-1)^{1-\alpha} < 12 - \bar{Z}$.
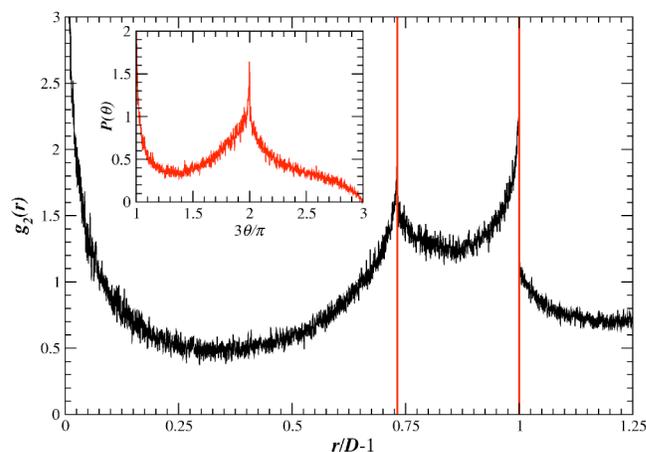
FIG. 9. (Color online) Computational data on the split-second peak of $g_2(r)$ averaged over five packings of 10 000 particles. The values $r = \sqrt{3}D$ and $r = 2D$ are highlighted and match the two observed discontinuities. Also visible is the divergence near contact. The inset shows the probability distribution $P_\theta(\theta)$ of bond-pair angles in the contact network of the packings, also revealing two divergences at $\theta = \pi/3$ and at $\theta = 2\pi/3$. No peaks are observed at $r = \sqrt{2}D$ or $r = \sqrt{5}D$, which are typical of crystal packings, indicating that there is no detectable crystal ordering in the packing.

first two coordination shells of the packing, and in fact observations have been made that along with the appearance of a peak in $P_f(f)$ for small forces, the splitting of the second peak of g_2 is a signature of jamming [29]. It is therefore important to try to understand the local geometrical patterns responsible for the occurrence of these structures in g_2.

4. Contact-network statistics

The exact geometry of the jammed configuration $\mathbf{R}_J$ is determined (not necessarily uniquely) from its contact network, which as we have demonstrated is the network of first-neighbor interactions and can easily be separated from further-neighbor interactions. Figure 10 shows the histogram of local coordination numbers as a function of the first-neighbor cutoff τ—i.e., the histogram of the number of particles within distance $(1+\tau)D$ from a given particle. It is seen that for sufficiently small τ ($\tau < 10^{-5}$) the histograms are independent of the exact cutoff used (this is true down to $\tau \approx 100\delta$ or so, which can be as small as 10^{-12} in some of our packings). It is interesting to observe that the contact-number probability distributions conform very well to a Gaussian shape, at discrete points between 4 and 10, for all of the cutoffs shown in the figure. A number of particles having fewer than two contacts are seen, and these are clearly *rattlers* and we have removed them from consideration from all of the final packings we analyze here. We observe that such particles remain with fewer than two contacts for a very wide range of τ and are easy to identify. In some cases, however, we cannot unambiguously identify a handful of the particles as rattlers or nonrattlers. This is typical for packings which are not sufficiently close to their jamming point, packings which have been produced using fast expansion in the LS algorithm, or packings which are very large. It is safest to not remove such particles as rattlers.

FIG. 10. (Color online) The probability distribution of local contact numbers as the cutoff used in defining neighbors is increased. Rattlers are clearly seen, and a relative maximum at $Z=6$ is seen. Note that only one particle with 11 neighbors is observed, and very few have as many as 10 neighbors. No particle with 12 contacting neighbors has been observed in any of our packings, indicating a lack of crystallinity.

This work is the first time a clear look has been provided at the exact contact network of disordered hard-sphere packings. Previous studies have either used soft atoms, in which case the definition of a contact is not clear cut unless one carefully takes limits of a stiff interaction potential [16], and therefore in such studies τ has been typically set to correspond to the location of the first minimum in $g_2(r)$ or have used Voronoi tessellations to define neighbors. Even studies which have actually used hard particles have resorted to such definitions unsuitable to investigating the jamming limit, mostly because the numerical precision required to separate the true contacts from the near contacts has not been achieved up to now [32]. Such investigations, the literature of which is too vast to cite, have found a plethora of local coordination patterns typical of *polytetrahedral* packing, including icosahedral order [32].

We therefore attempted to do a similar *shared-neighbor* [32] analysis for the contact networks of our disordered packings and look for local clusters reminiscent of polytetrahedral packing. Our procedure, based on looking at the contact network as an undirected graph, was as follows. For each particle, we extracted the subgraph corresponding to the first-neighbor shell of the particle (this includes contacts between the neighbors), extracted its connected components, and counted the number of occurrences of a given subgraph (using graph algorithms that can test for graph isomorphism to form equivalence classes). The results were surprising. By far the most prominent patterns were a central particle contacting a *chain* of 1, 2, 3, 4, or 5 contacting particles. The chains were almost never closed, other than for chains of length 3 (which together with the original particle form a contacting tetrahedron), and this was itself rare. The probability of finding a chain of length n seems to decay exponentially, $P(n) \sim \exp(-1.2n)$. This study found very few tetrahedra, and so polytetrahedral local ordering is certainly not apparent in the contact networks. We also performed the same analysis for a range of τ's, all the way up to $\tau=0.1D$ (which raises the average coordination significantly above 6), but still found the open linear chains to be the dominant pattern. We further attempted to include second neighbors in the analysis; however, including all second neighbors led to very large subgraphs of a very broad variety, so classification was not possible. We further restricted our attention only to second neighbors which are very close to the given particle (within $0.1D$, for example), and this also found very few tetrahedra.

One of our goals was to determine if certain simple local coordination patterns are responsible for each of the three features of $g_2(r)$ we previously documented: the power-law divergence near contact and the discontinuous, if not diverging, peaks at $r=\sqrt{3}D$ and $r=2D$. We had little success in accounting for the first one by restricting attention to only the first two neighbor shells in the true contact network. In particular, we looked at all the near contacts (for example, with gaps less than $0.01D$) and whether the almost contacting particles were in fact second neighbors in the contact network. Indeed, most were: however, the majority only shared one particle as a first neighbor or two or three first neighbors which were not themselves first neighbors. It was therefore not possible to isolate one particular local geometry as responsible for the multitude of near contacts. An interesting quantity we measured is the probability distribution $P_\theta(\theta)$ of bond-pair angles θ in the contact network, meaning the angles between two contact bonds of a given particle. This distribution is shown in the inset in Fig. 9 and shows divergences at $\theta=\pi/3$ and $\theta=2\pi/3$, which correspond to distances $r=2D\sin(\theta/2)$ of $r=D$ and $r=\sqrt{3}D$. Although there is no divergence at $\theta=\pi$, the corresponding distribution of distances does show a divergence at $r=2D$.

We had more success with a shared-neighbors analysis for the split second peak. This was because we could increase τ and thus progressively relax the definition of first neighbor. We found that with increasing τ, an increasing majority of particle pairs at a distance close to $\sqrt{3}D$ were second neighbors and that an increasing majority of them shared two neighbors which were themselves neighbors. This corresponds to two edge-sharing *approximately* equilateral coplanar triangles, a configuration which has been suggested as being responsible for the first part of the split-second peak [28]. Note, however, that we do not observe any discontinuity in g_2 at $r=1.633D$, which corresponds to two face-sharing tetrahedra, which is another configuration often mentioned in connection with the split-second peak. A similar analysis for the peak at $2D$ indicated that the majority of particle pairs at this distance share one neighbor between them, which represents an approximately linear chain of three particles, a configuration which has long been known to be responsible for the second part of the split-second peak of g_2.

B. Ordered packings

In this work we have focused on disordered hard-sphere packings and have found a multitude of unexpected singular features, such as a long power-law tail in $g_2^{(\delta)}(l)$, a nonzero $P_f(f=0)$, and a power-law divergence in $g_2^{(b)}(l)$. It is impor-
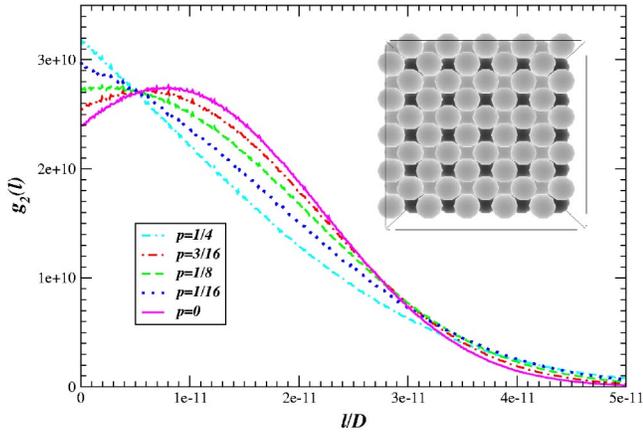
FIG. 11. (Color online) The first shell $g_2^{(\delta)}(l)$ for a collection of fcc crystal packings with a fraction p of the spheres removed, starting with $N=13\,500$ particles. The inset shows the packing with most vacancies, where every fourth sphere is removed to form a cubic sublattice of vacancies (colored dark). Intermediate p's are achieved by randomly adding back some of the spheres to the sublattice. The density has been reduced by $\delta = \sqrt{2} \cdot 10^{-11}$ from close packing.

tant to realize that the properties we observe are not universal and will change as one changes the amount of ordering of the packings. In particular, dense ordered packings like the fcc crystal are not isostatic, and we have no theory that can predict the shape of $g_2^{(\delta)}$. We therefore resort to a computational investigation of ordered and partially ordered sphere packings.

Vacancy-diluted fcc crystal packings

It was the behavior of crystal packings around the jamming point that was the subject of Refs. [3,4], and these
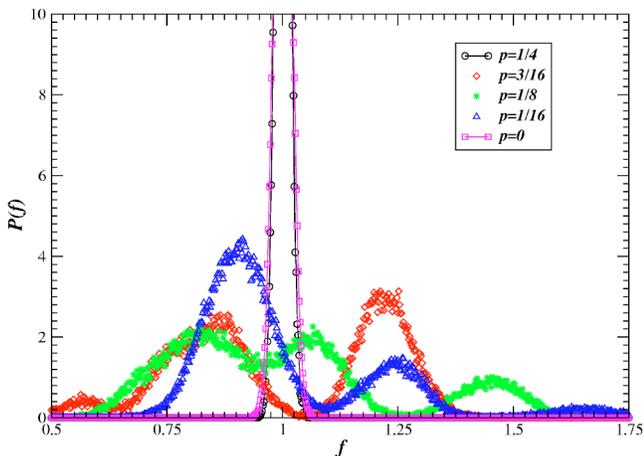
FIG. 12. (Color online) The force probability distribution for the collection of fcc crystal packings from Fig. 11. For the pure crystal and the crystal with the most vacancies, all of the particle pairs are identical and therefore the probability distribution would be a δ function if forces are averaged over an infinite time horizon. For the intermediate p's, multiple relatively broad peaks are observed. In contrast with the disordered case, very small forces are *not* observed.
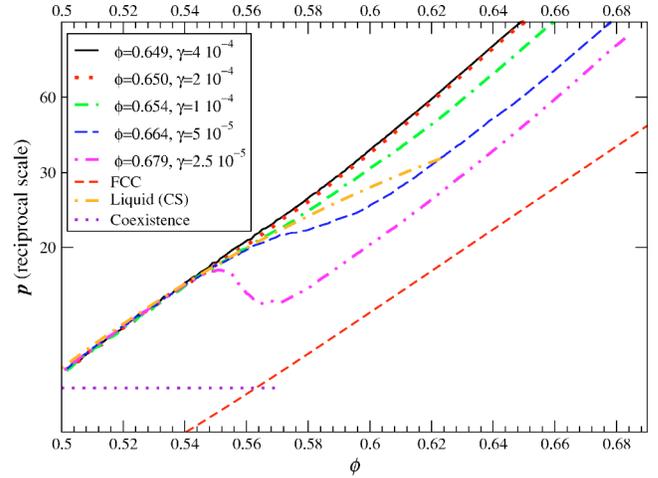
FIG. 13. (Color online) Compression of an initially liquid system with $\phi=0.5$ to jamming with several different expansion rates γ (the mean thermal velocity is 1, in comparison). The pressure is plotted on a reciprocal scale (the tickmarks being equally spaced in equal increments of p^{-1}, increasing in the usual direction), to highlight the expected linear relation (4) near jamming. The pressure-density curves for the perfect fcc crystal [23], the accepted fluid-solid coexistence region, and the widely known Carnahan-Starling equation of state for the fluid branch are also shown for comparison. Sufficiently fast compression suppresses crystallization and leads to densities around 0.64–0.65, and slower compression allows for partial crystallization, typically occurring around $\phi \approx 0.55$, which is the end of the coexistence region (i.e., the density where the crystal necessarily becomes thermodynamically favored). This produces denser packings which exhibit more crystal ordering the denser they are.

works inspired this investigation. For crystal packings, there is no ambiguity in defining first neighbors, and the fcc packing has $Z=12$ contacts per particle, which is twice the isostatic value. Therefore, the limiting polytope $\mathcal{P}_{\mathbf{x}}$ is not a simplex and, as argued in Ref. [4], it is expected that for an fcc packing $g_2^{(\delta)}(l)$ will have a single peak for small gaps. We indeed observe this computationally as shown in Fig. 11.

Furthermore, we have prepared vacancy-diluted fcc packings by removing a fraction p of the spheres from a perfect crystal, $0 \leq p \leq 4$ (here $p=0$ corresponds to the perfect crystal). The fcc lattice is composed of four interpenetrating cubic lattices. We obtain the vacancy-diluted crystal with the lowest density by removing one of these four cubic lattices (i.e., $p=1/4$), as shown in the inset in Fig. 11. This gives a packing with density of about $\phi \approx 0.56$ and mean coordination $\bar{Z}=8$ and is still collectively jammed. In fact, it is likely that more spheres can be removed with a more elaborate procedure [19]. We can add back a randomly chosen fraction $q=1/4-p$ of the previously removed quarter of the spheres to obtain $0 < p < 1/4$. The δ-function contributions to g_2 for several p's are shown in Fig. 11. It is rather surprising that the pair correlation function for the $p=1/4$ packing no longer shows a peak, but is monotonically decaying. In fact, by changing p one can obtain packings with $g_2^{(\delta)}(l)$ that has zero slope at the origin.

It is interesting to note that for the (vacancy-diluted) fcc packings $g_2^{(\delta)}(l)$ decays in a Gaussian manner and, in fact, is
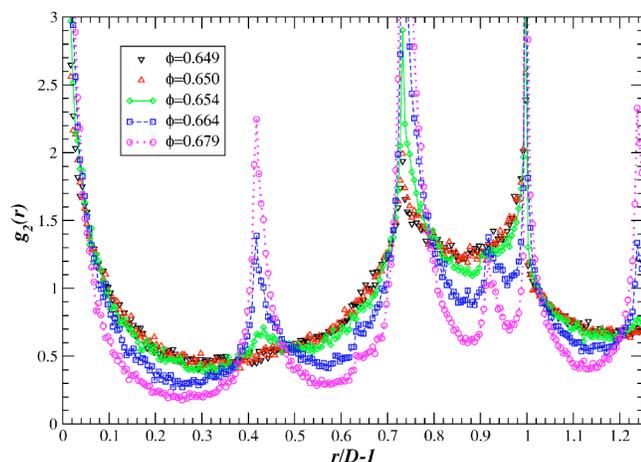
FIG. 14. (Color online) The evolution of the peaks in $g_2(r)$ as crystalline order is increased, for the packings from Fig. 13. The formation of peaks at distances typical of the fcc lattice, such as $r = \sqrt{2}$, is clearly seen. It is interesting to note that a peak is observed at $\sqrt{11/3} \approx 1.91$, which is a fifth-neighbor distance in the hcp (but not the fcc) lattice (a similar hcp peak at $\sqrt{8/3} \approx 1.63$ is barely visible). This is in agreement with numerous previous theoretical and numerical investigations of crystallization [33].

perfectly fitted by a modified Gaussian, $g_2^{(\delta)}(l) = (Al^2 + Bl + C)\exp[(l-D)^2]$. This fast decay is to be compared to the slow power-law decay for the disordered packings [cf. Eq. (9)], hinting at a possible connection to the stability of the crystal packings versus the metastability of the glass packings [10]. Additionally, we show the force distribution $P_f(f)$ for these ordered packings in Fig. 12, illustrating that, in contrast with the disordered packings, very small forces are not observed. It would be interesting to know if the perfect fcc crystal can be vacancy diluted to an isostatic packing and still be collectively or strictly jammed and what the corresponding force distribution would be.

C. Partially crystallized packings

As previously explained, the Lubachevsky-Stillinger algorithm can produce partially crystalline sphere packings if a sufficiently small expansion rate is used and nucleation of crystallites occurs during the densification. This is demonstrated in Fig. 13, where we show the evolution of the pressure during the densification of an initially liquid sample (i.e., a state on the stable equilibrium liquid branch) for a range of expansion rates γ. The slower the expansion is, the more crystalline the final packings become, as can be seen from the fact that the final density increases and from the evolution of the peaks in $g_2(r)$, as shown in Fig. 14. Additionally, the structure factor $S(\mathbf{k})$ shows more anisotropy and localized peaks. More detailed studies of crystallization using hard-sphere molecular dynamics have been performed by other researchers [10,33]. Here we are merely interested in how crystallization affects the properties we have studied in detail for the disordered packings.

The packings shown in Fig. 13 clearly have nucleated crystals, and so one may anticipate that there is a qualitative
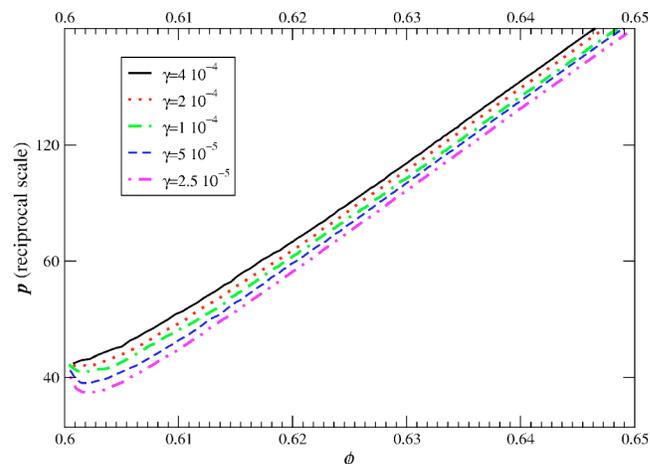
FIG. 15. (Color online) Compression of an initially (metastable) liquid system with $\phi = 0.6$ to jamming with several different expansion rates, as in Fig. 13. For this range of expansion rates, crystallization is suppressed due to the large initial density and all final packings are apparently disordered and would be ordinarily identified as random; however, it is clear that slower compression leads to higher densities, and thus the final packings are not all identical, but rather some are more ordered than others, as can be verified by the slight increase in bond-orientational order metric Q_6 [18], for example.

distinction between them and the "random" packings produced by suppressing crystallization. However, as demonstrated in Fig. 15, slower densification leads to larger densities and more ordered packings even if crystallization is suppressed and no visible nucleation occurs. This indicates that there is a continuum of packings from most disordered to perfectly ordered [18] packings, so that one needs to be careful in interpreting results obtained from packings produced by just one, possibly nontrivially biased, algorithm. For example, Ref. [29] relates the occurrence of a peak in $P_f(f)$ to jamming. However, as we show next, jammed packings do not necessarily exhibit this peak if they are sufficiently ordered.

For the sake of brevity, we will only briefly discuss some interesting features of g_2 for the partially crystallized packings. Since the perfect fcc or hcp crystals have $\bar{Z} = 12$, one expects that, as partial crystallization occurs, somehow the number of first neighbors per particle should increase from the isostatic value of $\bar{Z} = 6$. However, this is not really so if one *properly* defines first neighbors via true contacts in the final jammed packing. In fact, if one plots $Z(l)$ for partially crystallized packings (we omit this plot), a qualitatively similar curve to that shown in Fig. 6 is seen, with $\bar{Z}$ clearly close to the isostatic value of 6. However, the background $Z^{(b)}(l)$ shows a faster rise the more crystalline the packing is [consistent with a larger exponent α as defined in Eq. (10)], so that indeed an increase of the cumulative coordination is seen for sufficiently large gaps. Additionally, we observe that nearly crystalline packings easily jam in noticeably hypostatic configurations, with a higher probability of observing particles with only two or three contacts and a less flat plateau in $Z(l)$.
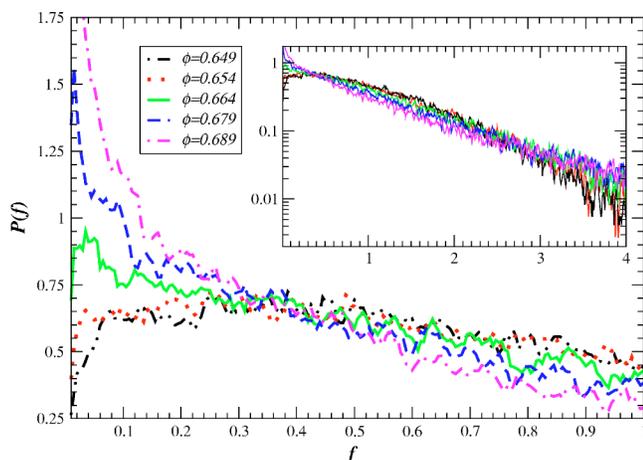
FIG. 16. (Color online) The evolution of $P_f(f)$ as crystalline order is increased, showing the disappearance of the peak at small forces. The inset shows a log-log view of the plot and is consistent with exponential decay for large forces.

All of these findings are readily explained. The basic premise, used widely in the granular media literature, is that random perturbations to either the particle-size distribution or to the boundary conditions will break some of the contacts in an otherwise perfect crystal down to the isostatic value. This is because additional contacts in excess of $\bar{Z}=6$ imply special correlations between the positions of the particles, which one expects to destroy with random perturbations. Such random perturbations are provided in the case of partially crystallized packings by the fact that the crystallites need to jam against a partially amorphous surroundings, and this induces complex strains that break some of the perfect-crystal contacts.[12] However, the geometric peculiarities of the underlying crystal remain; for example, there is a multitude of nearly collinear (in fact lines of aligned particles) or coplanar contacts, which leads to the occurrence of much more pronounced *force chains* (chains of large forces propagating along a nearly straight line) and a sharp increase in the probability of occurrence of small forces. We indeed observe this in Fig. 16, where we show that for sufficiently ordered packings there is no longer a peak in $P_f(f)$ for small forces, but rather a monotonic decrease of $P_f(f)$, apparently exponential for sufficiently large forces. This is in contrast to previous studies of the effect of order on force distributions in granular piles [34,35], which did not register a significant impact of the ordering. However, these studies examine the distribution of forces in granular piles and a direct comparison is beyond the scope of this work.

IV. DISCUSSION

The results presented in this work settle some long-standing questions and confusions in the literature. We showed both theoretically and computationally how the δ-function portion of $g_2(r)$ is formed as jamming is approached, for a true hard-sphere packing. Our investigation focused on maximally disordered (MRJ) sphere packings with a packing fraction $\phi \approx 0.64$–0.65. We presented true hard-sphere computational data on the power-law divergence in the near-contact portion of g_2, in agreement with previous observations in the literature for stiff soft spheres, but with a distinguishably different exponent of -0.4. We confirmed that this divergence persists even in the true jamming limit for hard particles. We presented high-quality data on the probability distribution of interparticle forces $P_f(f)$, especially focusing on small forces, demonstrating a maximum at small forces and a nonzero intercept at $f=0$. A local analysis of the topology of the contact network found few traces of tetrahedra and an overwhelmingly complex local connectivity and was successful in accounting for the structures responsible for the split-second peak of $g_2(r)$. A computational study of the δ-function contribution to $g_2(r)$ for vacancy-diluted fcc crystals showed a faster than exponential decay, unlike the slow power-law decay for the disordered isostatic packings. Finally, we investigated packings on the transition from maximally disordered to maximally ordered and found that partially crystallized packings produced by our algorithm are still nearly isostatic despite having a higher density and that $P_f(f)$ loses the peak for sufficiently ordered packings.

This work has raised several important questions. The computational observations undermine the very applicability of the ideal jammed packing model to large (maximally) disordered packings of spheres, as produced by most algorithms in use today. First, a very unusual power-law divergence in $g_2(l)$ is observed near contact, leading to a multitude of particle pairs just away from contact. Similarly, a power-law decay is seen in the contact part of $g_2(l)$. As the packings become larger, one can expect the tails of the two power laws to start overlapping by an observable number of contacts, blurring the distinction between true contacts and almost contacts. Even more troubling is the observation that there appears to be a positive probability of observing a zero force in the contact network of the packings, indicating the presence of geometric degeneracies in the contact network. The above observations may explain why we have had trouble generating truly jammed packings of $N=10\,000$ particles. However, we do not see a reason why very large but finite collectively jammed ideal packings could not be constructed. The question of what algorithm can produce disordered (and thus likely isostatic) packings which are jammed and devoid of some or all of the above peculiarities, as is the fcc crystal packing,[13] for example, remains open. As usual, with each careful study the hard-sphere system provides more questions than originally posed or answered.

---

[12]We mention in passing that we have observed similar results by starting with a perfect fcc crystal, applying a small (but not too small) random strain, and then jamming the packings. This typically yields almost perfectly crystal packings which are nonetheless clearly frustrated by the random strain to have $\bar{Z}\approx 6$.

---

[13]Note that the observations we list as troubling are separate from the rather general objections due to the inapplicability of the concept of ideal jamming to infinite packings, which apply to crystal packings as well [3].

[1] R. Zallen, *The Physics of Amorphous Solids* (Wiley, New York, 1983).

[2] S. Torquato, *Random Heterogeneous Materials: Microstructure and Macroscopic Properties* (Springer-Verlag, New York, 2002).

[3] Z. W. Salsburg and W. W. Wood, J. Chem. Phys. **37**, 798 (1962).

[4] F. H. Stillinger and Z. W. Salsburg, J. Stat. Phys. **1**, 179 (1969).

[5] A. Donev, S. Torquato, F. H. Stillinger, and R. Connelly, J. Comput. Phys. **197**, 139 (2004).

[6] S. Torquato and F. H. Stillinger, J. Phys. Chem. B **105**, 11 849 (2001).

[7] R. Connelly, Struct. Topol. **14**, 43 (1988); see also Ref. [36].

[8] R. Connelly, Invent. Math. **66**, 11 (1982).

[9] A. Donev, S. Torquato, F. H. Stillinger, and R. Connelly, J. Appl. Phys. **95**, 989 (2004).

[10] M. D. Rintoul and S. Torquato, Phys. Rev. Lett. **77**, 4198 (1996).

[11] A. Ferguson, B. Fisher, and B. Chakraborty, Europhys. Lett. **66**, 277 (2004).

[12] A. Donev, S. Torquato, and F. H. Stillinger, J. Comput. Phys. **202**, 737 (2005); **202**, 765 (2005).

[13] J. Brujic, S. F. Edwards, I. Hopkinson, and H. A. Makse, Physica A **327**, 201 (2003).

[14] S. F. Edwards and D. V. Grinev, Phys. Rev. Lett. **82**, 5397 (1999).

[15] H. A. Makse, J. Brujic, and S. F. Edwards, *The Physics of Granular Media* (Wiley, New York, 2004).

[16] L. E. Silbert, G. S. Grest, and J. W. Landry, Phys. Rev. E **66**, 061303 (2002).

[17] C. S. O'Hern, S. A. Langer, A. J. Liu, and S. R. Nagel, Phys. Rev. Lett. **88**, 075507 (2002).

[18] S. Torquato, T. M. Truskett, and P. G. Debenedetti, Phys. Rev. Lett. **84**, 2064 (2000).

[19] A. R. Kansal, S. Torquato, and F. H. Stillinger, Phys. Rev. E **66**, 041109 (2002); J. Chem. Phys. **117**, 8212 (2002).

[20] A. Donev, S. Torquato, F. H. Stillinger, and R. Connelly, Phys. Rev. E **70**, 043301 (2004).

[21] B. D. Lubachevsky and F. H. Stillinger, J. Stat. Phys. **60**, 561 (1990); see also Ref. [22].

[22] B. D. Lubachevsky, F. H. Stillinger, and E. N. Pinson, J. Stat. Phys. **64**, 501 (1991), second part of Ref. [21].

[23] R. J. Speedy, J. Phys.: Condens. Matter **10**, 4387 (1998).

[24] R. J. Speedy, Mol. Phys. **83**, 591 (1994).

[25] R. J. Speedy, J. Phys.: Condens. Matter **9**, 8591 (1997).

[26] T. Aste, M. Saadatfar, A. Sakellariou, and T. J. Senden, Physica A **339**, 16 (2004).

[27] L. E. Silbert, D. Ertas, G. S. Grest, T. C. Halsey, and D. Levine, Phys. Rev. E **65**, 031304 (2002).

[28] C. H. Bennett, J. Appl. Phys. **32**, 2727 (1972).

[29] C. S. O'Hern, S. A. Langer, A. J. Liu, and S. R. Nagel, Phys. Rev. Lett. **86**, 111 (2001).

[30] A. J. Liu, S. R. Nagel, D. A. Schecter, S. N. Coppersmith, S. Majumdar, O. Narayan, and T. A. Witten, Science **260**, 513 (1995).

[31] P. Metzger, Phys. Rev. E **70**, 051303 (2004).

[32] A. S. Clarke and H. Jonsson, Phys. Rev. E **47**, 3975 (1993).

[33] K. Kendall, C. S. F. van Swol, and L. V. Woodcock, Int. J. Thermophys. **23**, 175 (2002).

[34] D. L. Blair, N. W. Mueggenburg, A. H. Marshall, H. M. Jaeger, and S. R. Nagel, Phys. Rev. E **63**, 041304 (2001).

[35] J. H. Snoeijer, M. van Hecke, E. Somfai, and W. van Saarloos, Phys. Rev. E **67**, 030302(R) (2003).

[36] R. Connelly, Struct. Topol. **16**, 57 (1991), second part of Ref. [7].